Locally optimal law for maximum inclination change of a solar sail in an atmosphere

Valentin Stolbunov[1]
University of Toronto, Toronto, Canada, M3H 5T6.

Matteo Ceriotti[2], Camilla Colombo[3], and Colin R. McInnes[4]
University of Strathclyde, Glasgow, United Kingdom, G1 1XJ

The aim of this paper is to devise a local optimal strategy for orbital inclination change of solar sail spacecraft in low Earth orbit, combining the effects of the solar radiation pressure and atmospheric forces. The spacecraft is modeled as a reflective flat plate. The acceleration due to effects of atmospheric forces and solar radiation pressure is computed, depending on the orbital parameters and attitude of the sail. Then, the attitude that maximizes the instantaneous orbital inclination change is found through Gauss' equations. When either one of these effects dominates over the other (and so one can be neglected), analytic expressions are found. When both effects are considered, a numerical optimization is used. An additional constraint is introduced to avoid a decrease in orbital semi-major axis, and therefore prevent losses of orbital energy, while increasing the inclination. Different regions are identified, depending on whether the atmospheric effects dominate, the solar radiation pressure dominates, or the two are comparable. Arcs along the orbit are determined in which the optimal attitude can be found analytically, and the expression is derived. Numerical results show that a consistent increase of inclination can be achieved in a one year mission,

---

[1] MASc Candidate, University of Toronto Institute for Aerospace Studies, 4925 Dufferin Street. valentin.stolbunov@gmail.com.
[2] Currently at University of Glasgow, Systems Power and Energy division, School of Engineering, James Watt Building South, Glasgow G12 8QQ, Scotland, United Kingdom. Matteo.Ceriotti@glasgow.ac.uk. AIAA Member.
[3] Currently at University of Southampton, Astronautics Research Group, Faculty of Engineering and the Environment, Highfield, Southampton, United Kingdom, SO17 1BJ. c.colombo@soton.ac.uk. AIAA Member.
[4] Professor, Advanced Space Concepts Laboratory, Department of Mechanical and Aerospace Engineering, James Weir Building, 75 Montrose Street. colin.mcinnes@strath.ac.uk.

starting from different circular orbits, by applying the proposed control laws.

Nomenclature

a = Semi-major axis of spacecraft's orbit, km

$\mathbf{a}$ = Total non-gravitational acceleration, mm/s^2

a_0 = Characteristic acceleration of the solar sail spacecraft, mm/s^2

A = Spacecraft flat plate area, m^2

c_D = Coefficient of drag

c_L = Coefficient of lift

$\hat{\mathbf{D}}$ = Unit vector in the direction of aerodynamic drag

e = Eccentricity of spacecraft's orbit

f = True anomaly of spacecraft's orbit, deg or rad

h = Altitude of the orbit, km

$\mathbf{h}$ = Angular momentum vector per unit mass of spacecraft's orbit, km^2/s

i = Inclination of spacecraft's orbit, deg or rad

$\hat{\mathbf{L}}$ = Unit vector in the direction of aerodynamic lift

m = Spacecraft mass, kg

$\hat{\mathbf{N}}$ = Unit vector normal to the reflective flat plate

P = Local pressure on sail surface from photon momentum transport, N/m^2

$\mathbf{r}$ = Spacecraft position vector with respect to the center of the Earth, km

$\hat{\mathbf{r}}_{\mathbf{s}\odot}$ = Unit vector pointing from the spacecraft to the Sun, km

$\hat{\mathbf{t}}, \hat{\mathbf{n}}, \hat{\mathbf{h}}$ = Tangential, normal and out-of-plane right-handed reference frame, centered on the spacecraft

$\mathbf{v}, v$ = Velocity vector and its magnitude, km/s

v_b = Average normal thermal velocity of atmospheric particles in equilibrium with sail surface, km/s

α_N = Right ascension angle of the $\hat{\mathbf{N}}$ vector, deg or rad

$\alpha_\odot$ = Right ascension angle of the $\hat{\mathbf{r}}_{\mathbf{s}\odot}$ vector, deg or rad

β_N = Declination angle of the $\hat{\mathbf{N}}$ vector, deg or rad

$\beta_\odot$ = Declination angle of the $\hat{\mathbf{r}}_{\mathbf{s}\odot}$ vector, deg or rad

ζ = Angle complementary to flat plate's angle of attack, deg or rad

η = Solar sail efficiency factor

θ = Argument of latitude ($f + \omega$), deg or rad

$\lambda_\odot$ = Angle measured on the ecliptic between Sun position and direction of the gamma-point, deg or rad

μ = Gravity constant of the Earth, 3.9860×10^5 km^3/s^2

ρ = Atmospheric density, kg/m^3

σ_n = Accommodation coefficient for normal momentum exchange, 0.8

σ_t = Accommodation coefficient for tangential momentum exchange, 0.8

ϕ = Angle between pericenter of spacecraft's orbit and the direction of solar radiation, deg or rad

ω = Argument of the pericenter (measured from the ascending node) of spacecraft's orbit, deg or rad

Ω = Longitude of ascending node of spacecraft's orbit, deg or rad

Subscripts

opt = A vector or value which is deemed optimal

t, n, h = Components of vector quantities directed along the unit vectors of the $\hat{\mathbf{t}}, \hat{\mathbf{n}}, \hat{\mathbf{h}}$ frame

$aero$ = A vector or value resulting from the aerodynamic forces on the spacecraft

SRP = A vector or value resulting from the solar radiation pressure forces on the spacecraft

Superscripts

$+, -$ = Solution with "+" or "-"

I. Introduction

Solar sailing has for many years been an intriguing concept for spacecraft propulsion. The original concept has been studied extensively in the literature since its introduction during the beginning of the 1900's. The reason for this interest is mainly related to the capability of a solar sail to provide a continuous (albeit relatively small) acceleration, without using propellant mass. After many years of theoretical studies and laboratory experiments, JAXA's spacecraft IKAROS [1] successfully deployed the first solar sail in space, demonstrating that solar sailing is viable.

Most studies which focus on the use of solar sails are motivated by one of two types of space missions. The first of these are deep space interplanetary or Lagrange point missions [2]. The second type are high-altitude Earth bounded orbits where the effect of the atmosphere is negligible [3]. This is partly justified by the fact that a solar sail is a large surface of an extremely thin, membrane with

an extremely high area-to-mass ratio.

However, recently NASA's Nanosail-D2 [4] demonstrated the de-orbiting capabilities of a large, low-mass, high-surface area sail, also showing the feasibility of deploying a sail in the upper layers of the atmosphere, at least as a de-orbiting device. Nanosail-D2 was only passively stabilized by the atmospheric drag force on the sail and therefore could not be used to demonstrate solar sailing. Another demonstrator, CubeSail [5], is being designed and will be launched into a 800 km orbit with the aim of testing a 3-axis attitude control system. Despite its relatively low area-to-mass ratio, the mission will demonstrate the capabilities of a solar sail in a low Earth Sun-Synchronous orbit, where the sail is kept in a minimum-drag configuration.

The combined effects of solar radiation pressure (SRP) and aerodynamic forces are traditionally taken into account on spacecraft in low and medium Earth orbits in terms of perturbations on the dynamics of the spacecraft. Recently, Colombo et al. studied the effects of these forces on the long-term orbit evolution of large area-to-mass spacecraft such as a large solar sail or micro-scale 'SpaceChips,' considering a passively stabilised attitude [6]. It was shown that these effects can be exploited for orbit control, either modifying the reflectivity coefficient through electro-chromic coating to modulate the magnitude of the solar radiation pressure acceleration [7], or by engineering the drag coefficient by a change in temperature.

However, relatively little work has been done on exploiting these effects by actively changing the attitude of the spacecraft, with the aim of changing the orbital elements. In particular, if a large area-to-mass ratio spacecraft is modeled as a reflective plate subject to solar radiation pressure and aerodynamic forces, then its attitude can be controlled to substantially vary the two forces. The work of Morgan [8] investigated the use of a solar sail to increase the orbit inclination. In particular, the optimal roll angle of a solar sail that maintains a continuous no-drag configuration in a circular orbit was found. This results in no change in any of the Keplerian elements, except the inclination and the right ascension of the ascending node. More recent work by Mengali et al. [9] focused on the optimal control law of a solar sail spacecraft to increase the semi-major axis of a polar circular low Earth orbit.

The work presented here complements that of Mengali et al, in that the objective is to maximize

the orbital inclination change, with no decrease in semi-major axis (and therefore orbital energy).

After developing the dynamic model of the sail in a three-dimensional space, expressions for the acceleration due to both solar radiation pressure and aerodynamic forces are developed. Gauss' form of the Lagrange variational equations is then used to express the variation of the inclination and of the semi-major axis as a function of the attitude of the sail. Analytical solutions are found for maximizing the change of inclination in the two cases where either SRP or the aerodynamic force is dominant. It will be shown that, when the two effects are combined, and the constraint of non-decreasing semi-major axis is introduced, analytical solutions exist under certain conditions. In other cases, numerical methods have to be used. Finally, test case results will show the change of inclination that a spacecraft can potentially achieve in a year-long mission, starting from circular orbit at different altitude and considering moderate values for characteristic accelerations.

II. Dynamics model

In this section, the dynamics of the spacecraft, including the models of the solar radiation pressure (SRP) and aerodynamic forces will be outlined.

A spacecraft with a large, deployable surface, that can be modeled as a reflective flat plate, orbiting around the Earth (which is considered spherical uniform mass of radius 6378.16 km) is considered. The spacecraft's motion is subject to three accelerations: gravity, SRP and aerodynamic. Its motion can be modeled according to the following differential equation:

$$\ddot{\mathbf{r}} = -\frac{\mu}{r^2}\hat{\mathbf{r}} + \mathbf{a} \tag{1}$$

where $\mathbf{r}$ is the position vector of the spacecraft with respect to the Earth, $\mu = 3.9860 \cdot 10^5 \mathrm{km}^3/\mathrm{s}^2$ is the gravitational constant of the Earth and the 'dot' represents differentiation with respect to time. The vector $\mathbf{a}$ is the total, non-gravitational acceleration, and in this paper it is split into two contributions, one due to SRP and one due to atmospheric effects:

$$\mathbf{a} = \mathbf{a_{aero}} + \mathbf{a_{SRP}} \tag{2}$$

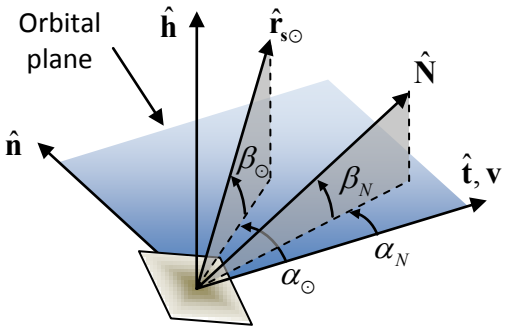

Fig. 1 The $\hat{\mathbf{N}}$ and $\hat{\mathbf{r}}_{s\odot}$ vectors in the $[t, n, h]^T$ frame.

The reference frame used in the following is centered on the spacecraft: the first axis, $\hat{\mathbf{t}}$, is aligned with the orbital velocity of the spacecraft $\dot{\mathbf{r}} = \mathbf{v}$ (and therefore tangent to the osculating orbit); the second axis, $\hat{\mathbf{n}}$, is normal to the velocity vector, in the orbital plane, and points in the direction of, but not necessarily directly at, the Earth; finally, the third axis, $\hat{\mathbf{h}}$, is normal to the orbital plane, aligned with the orbital angular momentum $\mathbf{h} = \mathbf{r} \times \mathbf{v}$, and completes the right-handed reference frame. Let us now consider a unit vector $\hat{\mathbf{N}}$, which defines the normal to the reflective flat plate, and therefore the attitude of the spacecraft, and a unit vector $\hat{\mathbf{r}}_{s\odot}$, which points from the spacecraft to the Sun (Fig. 1). Both these vectors are described through their yaw (α_N, $\alpha_\odot$) and pitch (β_N, $\beta_\odot$); right ascension is measured from the positive $\hat{\mathbf{t}}$ direction counterclockwise in the orbital plane, and declination is the out-of-plane angle, positive towards $\hat{\mathbf{h}}$. Therefore, it is clear that$\beta_N, \beta_\odot \in \left[-\frac{\pi}{2}, \frac{\pi}{2}\right]$ and $\alpha_N, \alpha_\odot \in [0, 2\pi]$. The vector components of $\hat{\mathbf{N}}$ and $\hat{\mathbf{r}}_{s\odot}$ are thus:

$$\hat{\mathbf{N}} = \begin{bmatrix} \cos\alpha_N \cos\beta_N \\ \sin\alpha_N \cos\beta_N \\ \sin\beta_N \end{bmatrix} \qquad \hat{\mathbf{r}}_{s\odot} = \begin{bmatrix} \cos\alpha_\odot \cos\beta_\odot \\ \sin\alpha_\odot \cos\beta_\odot \\ \sin\beta_\odot \end{bmatrix} \tag{3}$$

In the next subsections, the expressions for the acceleration due to the aerodynamic force and to the solar radiation pressure will be derived.

A. Aerodynamic acceleration

The spacecraft, modeled as a flat plate, is subject to an aerodynamic acceleration while moving through the atmosphere. The aerodynamic force, or acceleration, can be decomposed into lift (perpendicular to the velocity) and drag (opposite to the velocity):

$$\mathbf{a_{aero}} = \frac{1}{2}\rho v^2 \frac{A}{m}\left(c_L\hat{\mathbf{L}} + c_D\hat{\mathbf{D}}\right) \tag{4}$$

where c_L and c_D indicate respectively the coefficients of lift and drag, v is the spacecraft velocity with respect to the atmosphere, ρ is the local atmospheric density, A is the flat plate area, and m is the spacecraft mass. $\hat{\mathbf{L}}$ and $\hat{\mathbf{D}}$ are unit vectors along lift and drag, respectively.

Under hyperthermal flow conditions (translational velocity of solar sail much larger than thermal velocities of atmospheric particles) [9] an analytical expression of c_L and c_D can be used as defined in [10].

$$\begin{aligned} c_D &= 2\left(\sigma_t + \sigma_n\left(v_b/v\right)\cos\zeta + \left(2-\sigma_n-\sigma_t\right)\cos^2\zeta\right)\cos\zeta \\ c_L &= 2\left(\sigma_n\left(v_b/v\right) + \left(2-\sigma_n-\sigma_t\right)\cos\zeta\right)|\sin\zeta|\cos\zeta \end{aligned} \tag{5}$$

where σ_n and σ_t are the accommodation coefficients for normal and tangential momentum exchange, v_b is the average normal thermal velocity of the atmospheric particles which are in thermal equilibrium with the sail surface; in this paper, $\sigma_n = \sigma_t = 0.8$, $\frac{v_b}{v} = 0.05$ [9]. The angle $\zeta \in \left[-\frac{\pi}{2}, \frac{\pi}{2}\right]$ is complementary to the angle of attack of the flat plate:

$$\cos\zeta = |\hat{\mathbf{t}}\cdot\hat{\mathbf{N}}| \tag{6}$$

Note that in Eq. (6), the absolute value is used because the angle of attack is the same when $\hat{\mathbf{N}}$ is reflected. The absolute value in the term $|\sin\zeta|$ in Eq. (5), instead, is added because only in the magnitude of c_L is of interest as the sign of $c_L\hat{\mathbf{L}}$ will be adjusted later.

The component of the acceleration due to atmospheric drag is simply:

$$c_D\hat{\mathbf{D}} = -2\left(\sigma_t + \sigma_n\left(v_b/v\right)\cos\zeta + \left(2-\sigma_n-\sigma_t\right)\cos^2\zeta\right)\cos\zeta\hat{\mathbf{t}} \tag{7}$$

For the lift component, $c_L\hat{\mathbf{L}}$, it is required to derive an expression which is valid within the full space of possible orientations of the sail. The lift acceleration unit vector, $\hat{\mathbf{L}}$, is perpendicular to the velocity, and lies in the plane containing the velocity $\mathbf{v}$ and sail normal $\hat{\mathbf{N}}$. It follows that when $\hat{\mathbf{t}} \cdot \hat{\mathbf{N}} > 0$, $\hat{\mathbf{L}} = \frac{\hat{\mathbf{t}} \times (\hat{\mathbf{t}} \times \hat{\mathbf{N}})}{\|\hat{\mathbf{t}} \times \hat{\mathbf{N}}\|}$. However, the sign shall be adjusted in the case of $\hat{\mathbf{t}} \cdot \hat{\mathbf{N}} < 0$, to ensure that the flat plate produces the same lift when the normal switches direction with respect to the $\hat{\mathbf{t}}$ direction (see Fig. 2).

$$\hat{\mathbf{L}} = \mathrm{sgn}(\hat{\mathbf{t}} \cdot \hat{\mathbf{N}}) \frac{\hat{\mathbf{t}} \times (\hat{\mathbf{t}} \times \hat{\mathbf{N}})}{\|\hat{\mathbf{t}} \times \hat{\mathbf{N}}\|} \tag{8}$$

By noting that in Eq. (5) $|\sin\zeta| = \|\hat{\mathbf{t}} \times \hat{\mathbf{N}}\|$, the components of the acceleration due to atmospheric lift can be written as

$$c_L\hat{\mathbf{L}} = 2\left(\sigma_n\left(v_b/v\right) + \left(2 - \sigma_n - \sigma_t\right)|\hat{\mathbf{t}} \cdot \hat{\mathbf{N}}|\right)(\hat{\mathbf{t}} \cdot \hat{\mathbf{N}})(\hat{\mathbf{t}} \times (\hat{\mathbf{t}} \times \hat{\mathbf{N}})) \tag{9}$$

The full expression of the acceleration due to aerodynamic effects can be constructed from Eqs. (7), (9), and (3):

$$\mathbf{a_{aero}} = \frac{1}{2}\rho v^2 \frac{A}{m} \begin{bmatrix} -2\left|\cos\alpha_N\right|\cos\beta_N\left(\sigma_t + \sigma_n\left(v_b/v\right)\left|\cos\alpha_N\right|\cos\beta_N + \left(2 - \sigma_n - \sigma_t\right)\cos^2\alpha_N\cos^2\beta_N\right) \\ -2\cos\alpha_N\cos^2\beta_N\sin\alpha_N\left(\sigma_n\left(v_b/v\right) + \left(2 - \sigma_n - \sigma_t\right)\left|\cos\alpha_N\right|\cos\beta_N\right) \\ -2\cos\alpha_N\cos\beta_N\sin\beta_N\left(\sigma_n\left(v_b/v\right) + \left(2 - \sigma_n - \sigma_t\right)\left|\cos\alpha_N\right|\cos\beta_N\right) \end{bmatrix} \tag{10}$$

Eq. (10) describes all possible orientations of the sail in a three-dimensional space and ensures that two opposite directions of $\hat{\mathbf{N}}$, which corresponds to the same flat plate orientation, give the same $\mathbf{a_{aero}}$. This can be seen in Fig. 2 where for simplicity, the two-dimensional case is represented.

B. Solar radiation pressure acceleration

The reflective flat plate of the spacecraft is subject to the solar radiation pressure, and therefore acts as a solar sail. The attitude of the sail determines both the magnitude and direction of the

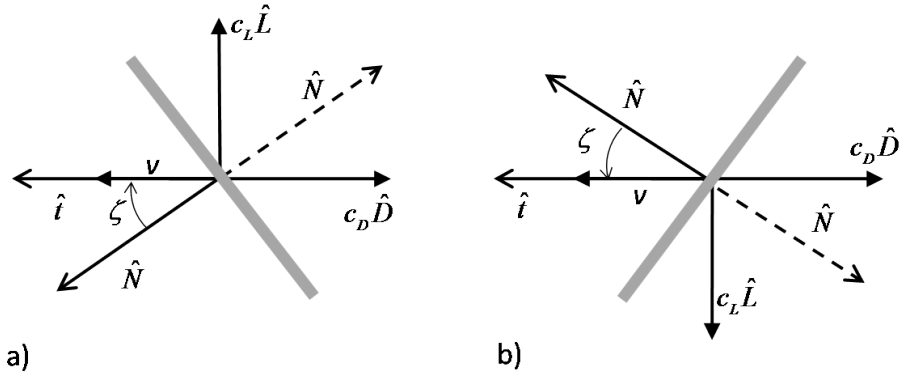

Fig. 2 Conventions for aerodynamic lift and drag a) lifting-plate and b) non-lifting plate

thrust obtained from the solar radiation pressure (SRP). If both sides of the solar sail are identical, the normal can be restricted to always point towards the Sun, that is

$$\hat{\mathbf{r}}_{\mathbf{s}\odot} \cdot \hat{\mathbf{N}} \geq 0 \tag{11}$$

the acceleration of a solar sail due to SRP in Earth's orbit is given as (see Ref. [11], pp. 39-40):

$$\mathbf{a_{SRP}} = -a_0(\hat{\mathbf{r}}_{\mathbf{s}\odot} \cdot \hat{\mathbf{N}})^2\hat{\mathbf{N}} \tag{12}$$

where a_0 is the characteristic acceleration of the sail, i.e.

$$a_0 = \frac{2\eta PA}{m} \tag{13}$$

where P is the local pressure exerted on the surface due to momentum transport by photons ($P \approx 4.56 \times 10^{-6}\,\mathrm{Nm}^{-2}$ at 1 AU, and considered constant), and $\eta = 0.85$ is a factor that takes into account the non-perfect reflectivity of the sail. Note also that the characteristic acceleration is proportional to the area-to-mass ratio of the spacecraft. The constraint in Eq. (11) allows $\hat{\mathbf{N}}$ to point in one half of the local 3D space and, due to the sail's flat plate nature and symmetry of atmospheric effects, covers all possible orientations of the sail and thus all possible combinations of atmospheric and SRP forces. By substituting the expression of $\hat{\mathbf{N}}$ and $\hat{\mathbf{r}}_{\mathbf{s}\odot}$ in terms of the sail and Sun angles, as defined in Eq. (3), and with some trigonometric manipulations, the full expression for the sail acceleration due to solar radiation pressure is

$$\mathbf{a_{SRP}} = -a_0 \left[\cos\beta_\odot \cos\beta_N \cos(\alpha_\odot - \alpha_N) + \sin\beta_\odot \sin\beta_N\right]^2 \begin{bmatrix} \cos\alpha_N \cos\beta_N \\ \sin\alpha_N \cos\beta_N \\ \sin\beta_N \end{bmatrix} \tag{14}$$

III. Maximization of inclination change

Now that the forces acting on the spacecraft have been modeled, locally optimal control laws to maximize the change of inclination at any given instant of time shall be investigated. This means finding the optimal attitude of the spacecraft (i.e. α_N, β_N) as a function of its osculating orbital elements and relative position of the Sun.

As mentioned, the spacecraft is subject to the gravitational acceleration of the Earth, which is considered a point mass, and to the SRP and atmospheric accelerations. Therefore, the change in Keplerian orbital elements due to the non-gravitational accelerations can be expressed with the Gauss' form of Lagrange's variational equations of planetary motion [12]. In particular, the instantaneous change in orbit inclination i is given as:

$$\frac{di}{dt} = \frac{r\cos\theta}{h} a_h \tag{15}$$

with $\theta = f + \omega$, where f is the true anomaly (measured from pericenter) and ω the argument of the pericenter (measured from the ascending node). h is the orbit angular momentum and a_h is the out-of-plane acceleration.

In order to maximize the change in orbit inclination, the goal is then to maximize the third component (out of plane) of the acceleration vector in Eq. (2) when $\cos\theta > 0$, and minimize it when $\cos\theta < 0$. Stationary points can be found by solving the following system involving first-order derivatives of a_h with respect to the sail angles α_N, β_N:

$$\begin{cases} \dfrac{\partial a_h}{\partial \alpha_N} = 0 & \text{(16a)} \\ \dfrac{\partial a_h}{\partial \beta_N} = 0 & \text{(16b)} \end{cases}$$

However, the variation in semi-major axis cannot be neglected. In fact, in most of the cases, while a change of inclination is needed, this shall not be achieved at the expense of a decrease in orbital energy. Therefore, the case in which the change of inclination is maximized, with the constraint of the change in semi-major axis to be positive or at most null, is investigated.

Referring again to the Gauss' equations, the instantaneous change in semi-major axis a is given as:

$$\frac{da}{dt} = \frac{2a^2 v}{\mu} a_t \tag{17}$$

where a_t is the tangential acceleration. Therefore in order to never have $\frac{da}{dt} < 0$, the solution is subject to the constraint:

$$a_t \geq 0 \tag{18}$$

Before studying the complete case with SRP and aerodynamic acceleration from Eq. (2), it is useful to analyze the cases in which either only SRP or aerodynamic acceleration is present, as analytical solutions are available for these simplified cases. The case of acceleration dominated by SRP and acceleration dominated by atmospheric effects will be addressed in the next subsections.

A. SRP-dominated case

This case occurs at high altitude, where $\rho \approx 0$. As a result, the expression for the total acceleration can be approximated with Eq. (14), and the out-of-plane component is:

$$a_{SRP,h} = -a_0 \sin\beta_N \left[\cos\beta_\odot \cos\beta_N \cos(\alpha_\odot - \alpha_N) + \sin\beta_\odot \sin\beta_N\right]^2 \tag{19}$$

For this case, an analytical solution exists. Developing Eq. (16a) with the expression in Eq. (19):

$$-2a_0 \sin\beta_N \left[\cos\beta_\odot \cos\beta_N \cos(\alpha_\odot - \alpha_N) + \sin\beta_\odot \sin\beta_N\right] \cos\beta_\odot \cos\beta_N \sin(\alpha_\odot - \alpha_N) = 0 \tag{20}$$

which has the following two solutions for α_N:

$$\cos(\alpha_N - \alpha_\odot) = -\tan\beta_\odot \tan\beta_N \tag{21a}$$

$$\alpha_N = \alpha_\odot \tag{21b}$$

Developing the other derivative (Eq. (16b)):

$$\cos\beta_N \left[\cos\beta_\odot \cos(\alpha_\odot - \alpha_N)\cos\beta_N + \sin\beta_\odot \sin\beta_N\right] = 2\sin\beta_N \left[\cos\beta_\odot \cos(\alpha_\odot - \alpha_N)\sin\beta_N - \sin\beta_\odot \cos\beta_N\right] \tag{22}$$

Solving for $\tan\beta_N$ (see Appendix VI A for full development):

$$\tan\beta_N = \frac{3\tan\beta_\odot \pm\sqrt{9\tan^2\beta_\odot + 8\cos^2(\alpha_\odot - \alpha_N)}}{4\cos(\alpha_\odot - \alpha_N)} \tag{23}$$

Note that this equation is the solution found by Morgan [8]. In that work, the angle named here as α_N was fixed to $-\frac{\pi}{2}$ to have null aerodynamic drag.

Solutions to the system in Eq. (16) for SRP only can be found by inserting either solution in Eq. (21a) or Eq. (21b) into Eq. (23). The first gives a non-acceptable solution (see Appendix VI A), while the second leads to

$$\begin{cases} \alpha_N = \alpha_\odot \\ \tan\beta_N = \frac{3\tan\beta_\odot \pm\sqrt{9\tan^2\beta_\odot + 8}}{4} \end{cases} \tag{24}$$

These are therefore the only two solutions, and they are not defined for $\beta_\odot = \pm\pi/2$. It is now important to show that the two stationary points in Eq. (24) are the maximum and the minimum of $a_h(\alpha_N, \beta_N)$, and identify them.

First of all, note that for any $-\pi/2 < \beta_\odot < \pi/2$, $\frac{3\tan(\beta_\odot)+\sqrt{9\tan^2(\beta_\odot)+8}}{4} > 0$, and $\frac{3\tan(\beta_\odot)-\sqrt{9\tan^2(\beta_\odot)+8}}{4} < 0$. This means that, for the "+" solution, $\beta_N > 0$ and thus, from Eq. (19), $a_h < 0$. In the same way, for the "-" solution, $\beta_N < 0$ and thus $a_h > 0$.

The extreme value theorem states that if a function is defined on a closed and bounded domain and is continuous there, then it is either constant, or it attains its maximum and minimum in that set. If the function is also differentiable, then the extrema can either be at stationary points inside the domain, or on the bound of the domain (not necessarily at stationary points). For the case of $a_h(\alpha_n, \beta_N)$, let us consider the bounds first. The bounds of the domain are defined by $\alpha_N \in [0, 2\pi], \beta_N \in \left[-\frac{\pi}{2}, \frac{\pi}{2}\right]$ and by the nonlinear Sun-sail constraint (Eq. (11)). Now, if extrema of a_h are on the first type of bound, then they shall be on a stationary point, since a_h is periodic and the whole period is considered. Instead, the extrema could be on the nonlinear bound, however this is not the case, since it is easy to see that on that bound $a_h = 0$, and a_h is positive on one stationary point and negative on the other one. Therefore the extrema must be inside the domain, at a stationary point. With only two stationary points present, one positive and one negative, it can be concluded that the "+" solution represents the minimum out-of-plane acceleration (and negative), while the "-" solution is the maximum out-of-plane acceleration (and positive).

By observing the squared term in the square brackets of Eq. (19), it can be stated that, if the Sun is above the orbital plane ($\beta_\odot > 0$), the maximum downward out-of-plane acceleration would have a higher magnitude than the maximum upward one. Similarly with the Sun below the plane, an upward a_h would be of greater magnitude. In fact, $\alpha_N = \alpha_\odot$ (for optimality), $\cos\beta_\odot \cos\beta_N > 0$, and the term $\sin\beta_\odot \sin\beta_N$ contributes positively if $\sin\beta_\odot$ and $\sin\beta_N$ have the same sign. Hence, the maximum absolute value of acceleration can only be achieved when the Sun is in a favorable relative position. In any case, to maximize the inclination change, the required alternation between $a_h > 0$ and $a_h < 0$ (as mentioned earlier) is achieved through switching between the positive and negative solutions.

Furthermore, the same solution in Eq. (24) can be obtained in terms of cone and clock angle of the sail with respect to the Sun vector by following the procedure described in [11] pp. 115-116.

Finally, as remarked, the derived solutions (Eq. (24)) are not defined in the case of $\beta_\odot = \pm\pi/2$, when the Sun vector is perpendicular to the orbital plane, which can happen for a highly inclined orbit. In this case, the solutions can be found considering a limit analysis (see Appendix VI A). It results in:

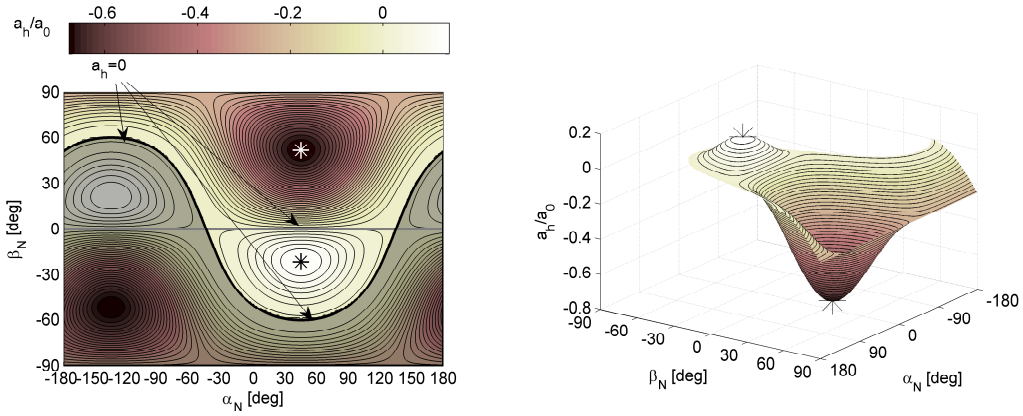

(a) (b)

Fig. 3 $a_{SRP,h}/a_0$ as function of α_N and β_N. The Sun is located at $\alpha_\odot = \frac{\pi}{4}, \beta_\odot = \frac{\pi}{6}$. (a) Contour plot. The unfeasible region due the Sun-sail constraint is shaded; (b) Three-dimensional view. The unfeasible region in not plotted.

$$\begin{aligned} \beta_\odot = \tfrac{\pi}{2} : & \begin{cases} \arg\max_{\beta_N}(a_h) = 0, a_h = 0 \\ \arg\min_{\beta_N}(a_h) = \frac{\pi}{2} \end{cases} \\ \beta_\odot = -\tfrac{\pi}{2} : & \begin{cases} \arg\max_{\beta_N}(a_h) = 0 \\ \arg\min_{\beta_N}(a_h) = \frac{\pi}{2}, a_h = 0 \end{cases} \end{aligned} \tag{25}$$

As an example, the function $a_{SRP,h}(\alpha_N, \beta_N)$ is plotted in Figure 3 for a specific solar sail and position of the Sun with respect to the orbit. The domain in which the function exists is defined by the nonlinear Sun-sail constraint (Eq. (11)). Both extrema are visible and because the Sun is above the sail ($\beta_\odot > 0$) the maximum upward out-of-place acceleration is significantly less than the maximum downward acceleration. Figure 3 represents the out-of-plane acceleration $a_{SRP,h}$ (normalized with respect to a_0) as function of α_N and β_N, for a specific position of the Sun. The shaded area in the figure represents the domain in which $\hat{\mathbf{r}}_{\mathbf{s}\odot} \cdot \hat{\mathbf{N}} < 0$ according to constraint Eq. (11). The maximum and minimum solutions for the out-of-plane acceleration, as given by Eq. (24) are marked in the plots with a star.

Let us now study Eq. (18). The expression for the tangential acceleration is:

$$a_{SRP,t} = -a_0 \cos\alpha_N \cos\beta_N \left[\cos\beta_\odot \cos\beta_N \cos(\alpha_\odot - \alpha_N) + \sin\beta_\odot \sin\beta_N\right]^2 \tag{26}$$

This expression is positive if:

$$\cos\alpha_N \cos\beta_N \leq 0 \tag{27}$$

From Eq. (3), this condition can be rewritten as:

$$\hat{\mathbf{N}} \cdot \hat{\mathbf{t}} \leq 0 \tag{28}$$

This is justified noting that the solar sail acceleration is directed opposite to its normal, and the velocity vector is directed as $\hat{\mathbf{t}}$. In this way, the solar sail acceleration always has a positive, or at least null, component towards the velocity vector.

Figure 4 represents the tangential SRP acceleration $a_{SRP,t}$ as function of α_N and β_N. Also in this case, it is normalized with respect to a_0, and the shaded area represents the unfeasible domain constrained by Eq. (11). The black bold lines represent the sail orientation for which $a_{SRP,t} = 0$. The constraint Eq. (28) is verified only in the domains at the top left and top right of the plot.

B. Atmospheric-effect-dominated case

The case in which the effect of SRP can be neglected, and only the atmospheric force is taken into account, models a spacecraft in an orbit of low altitude, such that $\rho v^2 \gg 4\eta P$. The result is a flat plate orbiting the Earth with an out-of-plane acceleration that is independent of the Sun's location and given by:

$$a_{aero,h} = \frac{1}{2}\rho v^2 \frac{A}{m} \left(-2\cos\alpha_N \cos\beta_N \sin\beta_N \left(\sigma_n \left(v_b/v\right) + \left(2 - \sigma_n - \sigma_t\right) \left|\cos\alpha_N\right| \cos\beta_N\right)\right) \tag{29}$$

The magnitude of acceleration in the $\hat{\mathbf{h}}$ direction can be maximized with respect to (α_N, β_N), as shown in detail in Appendix VI B, to give

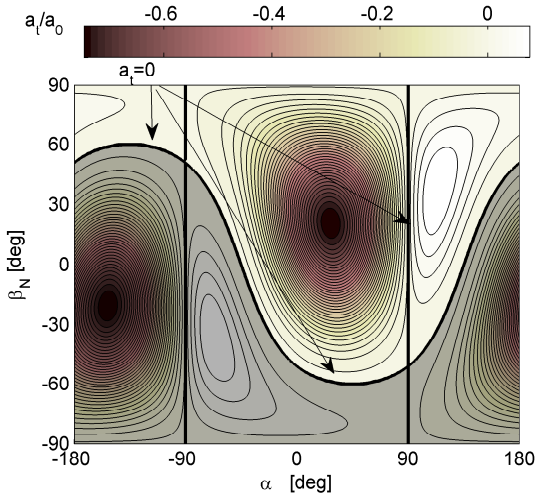

Fig. 4 Contour plot of $a_{SRP,t}/a_0$ as function of α_N and β_N. The Sun is located at $\alpha_\odot = \frac{\pi}{4}, \beta_\odot = \frac{\pi}{6}$. The unfeasible region due the Sun-sail constraint is shaded.

$$\begin{cases} \alpha_{N,opt} = 0, \pi & \text{(30a)} \\ \beta_{N,opt} = & \\ \pm \arccos\left(\frac{2}{9(2-\sigma_n-\sigma_t)} \left(-\sigma_n \left(v_b/v\right) + \sqrt{2\left(9\left(2-\sigma_n-\sigma_t\right)^2 + 2\left(\sigma_n\left(v_b/v\right)\right)^2\right)} \cdot \cos\frac{\chi}{3} \right) \right) & \text{(30b)} \end{cases}$$

where χ is given by:

$$\chi = \arctan \frac{9\left(2-\sigma_n-\sigma_t\right)\sqrt{288\left(2-\sigma_n-\sigma_t\right)^4 - 33\left(2-\sigma_n-\sigma_t\right)^2\left(\sigma_n\left(v_b/v\right)\right)^2 + 96\left(\sigma_n\left(v_b/v\right)\right)^4}}{135\left(2-\sigma_n-\sigma_t\right)^2\left(\sigma_n\left(v_b/v\right)\right) - 16\left(\sigma_n\left(v_b/v\right)\right)^3} \tag{31}$$

The out-of-plane component of the acceleration due to atmospheric forces $a_{aero,h}$ is shown in Fig. 5 ($a_{aero,h}$ is normalized with respect to $\frac{1}{2}\rho v^2 \frac{A}{m}$). As expected from the third component of Eq. (10), $a_{aero,h}$ is symmetric around $\alpha_N = 0$ and anti-symmetric around $\beta_N = 0$. The solutions (α_N, β_N) for $\max|a_{aero,h}|$ are represented with the star symbols. It is found that the magnitude of the out-of-plane component of acceleration is maximized at an angle of attack of about $\pm 54°$. It is worthwhile to note that the two maxima for $a_{aero,h}$ at $(0, \beta^-_{N,opt})$ and $(\pi, \beta^+_{N,opt})$, where $\beta^+_{N,opt}$ and $\beta^-_{N,opt}$ are respectively the positive and negative solution of Eq. (30b), represent the same sail orientation with respect to the incoming particles of the atmosphere (the normal to the sail is in opposite directions). The same observation is valid for the two minima at $(0, \beta^+_{N,opt})$ and $(\pi, \beta^-_{N,opt})$.

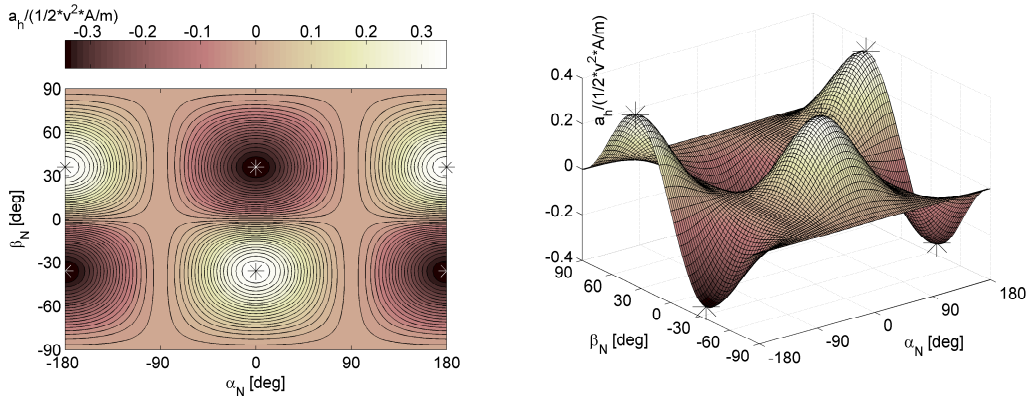

(a) (b)

Fig. 5 Normalized $a_{aero,h}$ as function of α_N and β_N for a flat plate subject only to atmospheric force. (a) Contour plot; (b) Three-dimensional view.

Regarding the tangential acceleration, the constraint in Eq. (18) can be satisfied only if $a_{aero,t} = 0$ as in the first component of Eq. (10)

$$a_{aero,t} = -\rho v^2 \frac{A}{m} |\cos\alpha_N| \cos\beta_N \left(\sigma_t + \sigma_n \left(v_b/v\right) |\cos\alpha_N| \cos\beta_N + \left(2 - \sigma_n - \sigma_t\right) \cos^2\alpha_N \cos^2\beta_N\right) \tag{32}$$

where the last term in parenthesis is always positive and $|\cos\alpha_N| \cos\beta_N$ is positive or null, hence the only way to satisfy the constraint is $a_{aero,t} = 0$. This is verified if

$$\alpha_N = \pm\frac{\pi}{2} \tag{33}$$

or

$$\beta_N = \pm\frac{\pi}{2} \tag{34}$$

Equations. (33) and (34) represent the trivial solution of a sail at zero angle of attack. Figure 6 represents the tangential acceleration as function of α_N and β_N. Also in this case $a_{aero,t}$ is normalized with respect to $\frac{1}{2}\rho v^2 \frac{A}{m}$.

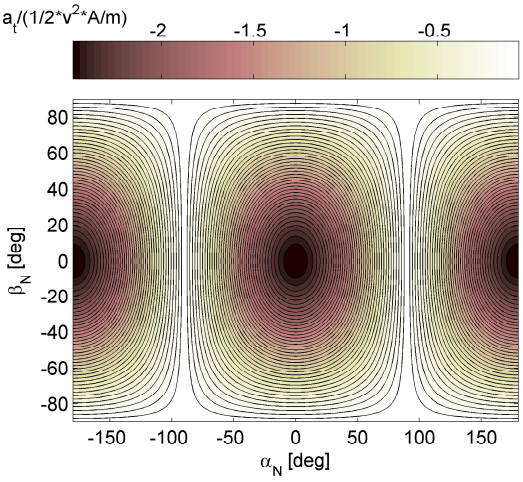

Fig. 6 Normalized $a_{aero,t}$ as function of α_N and β_N for a flat plate subject only to atmospheric effects.

C. Combined SRP and atmospheric-effect acceleration

In this section, the effect of combining the two acceleration contributions is analyzed, as well as the non-linear constraints Eq. (11) and Eq. (18).

In the presence of both SRP and atmospheric effects, the solution for maximizing the change of inclination under the non-linear constraints could not be found analytically. The solution is then determined numerically through a global search using a multi-start technique. 1000 randomly distributed starting points in the range of $\beta_N \in \left[-\frac{\pi}{2}, \frac{\pi}{2}\right]$ and $\alpha_N \in [0, 2\pi]$ are sampled, and a local constrained optimization is started from each feasible point. The algorithm is implemented in MATLAB functions *MultiStart* and *fmincon*.

Figure 7 shows two contour plots of the full out-of-plane and tangential acceleration respectively, a_h and a_t, functions of α_N, β_N. For this figure a solar sail with $a_0 = 0.2\,\mathrm{mm/s^2}$ is considered and the Sun is located at $\alpha_\odot = \frac{\pi}{4}$, $\beta_\odot = \frac{\pi}{6}$. The reason for considering a smaller value of the sail characteristic acceleration with respect to the range considered in Mengali et al. [9] is explained in Section V. The figure refers to a circular orbit around the Earth ($v = \sqrt{\mu/r}$) at an altitude $h = 700$ km and from Eq. (13), $\frac{A}{m} = 25.79\,\mathrm{m^2/kg}$ hence $0.5\rho v^2 A/m = 2.63 \cdot 10^{-2}\,\mathrm{mm/s^2}$. An exponential model for the atmospheric density with altitude is used [13]. At the altitude considered here, neither of the two contributions is negligible with respect to the other. The two non-linear

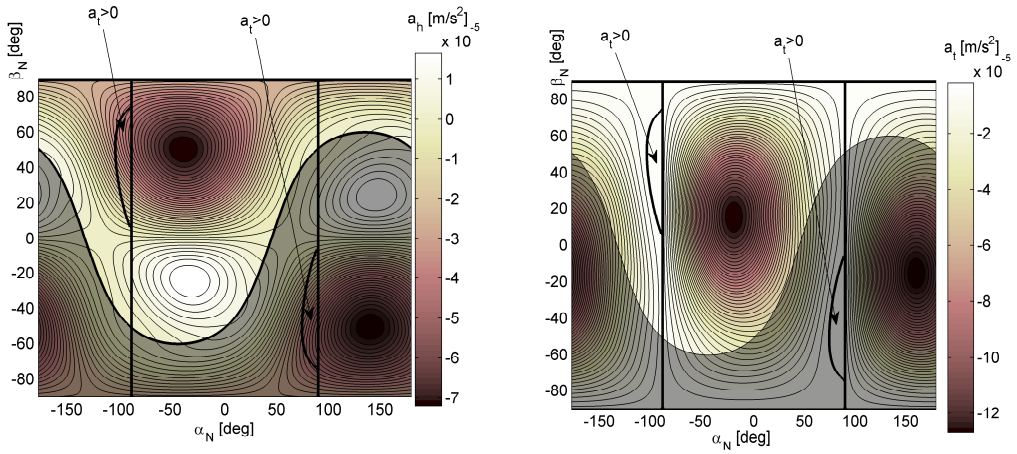

(a) (b)

Fig. 7 Contour plot of a_h and a_t as function of α_N and β_N. Circular orbit at 700 km altitude; the Sun is located at $\alpha_\odot = \frac{\pi}{4}, \beta_\odot = \frac{\pi}{6}$. The unfeasible region due the Sun-sail constraint is shaded and the region with $a_t > 0$ is indicated with arrows

constraints in Eq. (11) (Sun-sail pointing) and Eq. (18) (semi-major axis change) are represented in the plots. In particular the shaded area shows the unfeasible region due to the Sun-sail pointing, while the semi-major axis constraint defines the two disconnected regions indicated with the arrow. In this particular case, the semi-major axis constraint removes a significant portion of the search space, and the maximum out-of-plane acceleration value is considerably affected by this constraint.

Figure 8 shows the results of the optimization process for a circular orbit at 700 km, and different relative positions of the Sun. Figure 8(a) shows the maximum attainable a_h (optimal solution) for each value of the combination $\alpha_\odot$ and $\beta_\odot$, while Fig. 8(b) shows the corresponding a_t at the same angles. It is worth noting that there will always be a sail orientation which will have $a_t \geq 0$ and $a_h \geq 0$ (or $a_h \leq 0$). The worst possible case for a_t is with the Sun directly in front of the sail ($\beta_\odot = 0, \alpha_\odot = 0$), such that $\hat{\mathbf{r}}_{\mathbf{s}\odot} = \hat{\mathbf{t}}$ and it is not possible take advantage of the solar radiation pressure to have $a_t > 0$ and therefore increase the semi-major axis. In this case, any $\hat{\mathbf{N}}$ such that $\hat{\mathbf{t}} \cdot \hat{\mathbf{N}} = 0$ will ensure a flat plate traveling with zero drag and provide $a_t = 0$. In the worst possible case for a maximum a_h, the Sun is directly above the orbital plane ($\beta_\odot = \pi/2$) such that it is not possible to generate any $a_h > 0$ with the SRP. In this case, the atmospheric effects can be used to generate lift. If the atmospheric effect is insignificant, then the sail can be positioned such that

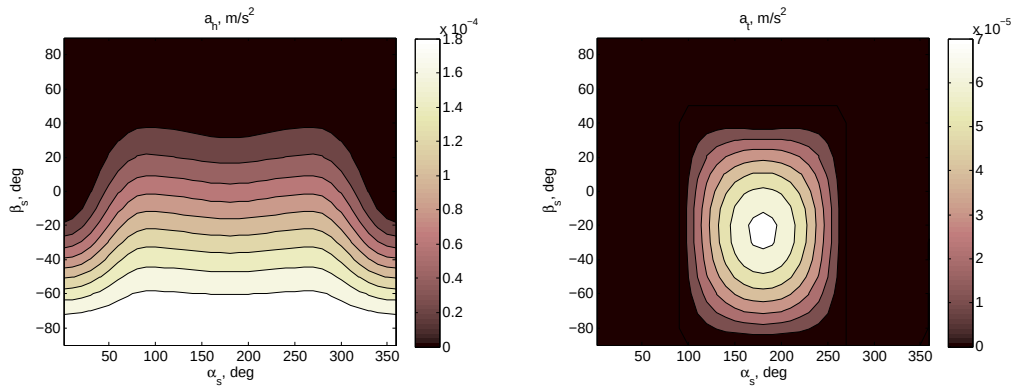

(a) (b)

Fig. 8 Maximum attainable a_h (a) and a_t (b) function of $\alpha_\odot, \beta_\odot$ for a sail ($a_0 = 0.2\,\mathrm{mm/s^2}$) subject to both SRP and atmospheric effects on a 700-km-altitude circular orbit. Sail is constrained to maintain $a_t \geq 0$ and Sun pointing.

$\hat{\mathbf{r}}_{\mathbf{s}\odot} \cdot \hat{\mathbf{N}} = 0$ and provide $a_h = 0$. Depending on the relative strength of the two types of accelerations, the best option may be a sail orientation such that both $\hat{\mathbf{t}} \cdot \hat{\mathbf{N}} = 0$ and $\hat{\mathbf{r}}_{\mathbf{s}\odot} \cdot \hat{\mathbf{N}} = 0$. This would result in $a_h = a_t = 0$ and it is the worst possible case.

Note that, at this altitude, the maximum value of a_h is greatest when the Sun is best able to contribute to the out-of-plane acceleration by being directly below the sail ($\beta_\odot = -\frac{\pi}{2}$). As the Sun angle increases, however, there is a decrease in maximum attainable a_h until $a_h \approx 0$ for most values of $\alpha_\odot$ at $\beta_\odot \geq \frac{\pi}{4}$. At these high values of $\beta_\odot$ the sail normal is essentially aligned perpendicular to the Sun-line vector to avoid a downward out-of-plane acceleration from the solar radiation pressure.

Now, observing Fig. 9, the region of $a_t > 0$ is largely around the $\alpha_\odot = \pi$ line when the Sun is behind the satellite and solar radiation pressure can directly contribute to an acceleration in the positive $\hat{\mathbf{t}}$ direction. In this region the satellite can attain its maximum a_h as no compromise has to be made in terms of sail attitude to keep $a_t \geq 0$. Out of this region however, the a_t plot is flat at 0 and the sail cannot obtain its maximum out-of-plane acceleration as it is constrained to keep $a_t \geq 0$.

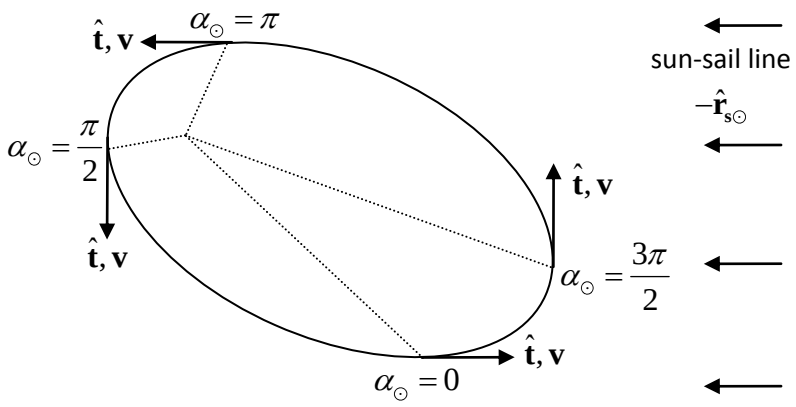

Fig. 9 Definition of $\alpha_\odot$ angles and the Sun direction for an arbitrary orbit.

IV. Optimal solution regions

It was noted earlier that an analytic expression is not found for the general case where the two effects are combined and the constraints are satisfied. Nevertheless, the following sections provide some further insight on the optimal attitude in different conditions.

The first observation is related to the altitude of the spacecraft: it is expected that, at very low altitude, the effect of the atmosphere would be more dominant than that of SRP, and therefore the optimal solution will be close to the atmospheric-only solution. However, the sole atmospheric-only solution that is compatible with the semi-major axis constraint is the one that produces no drag and no lift. In this solution, $\alpha_N = \pi/2, 3\pi/2$ as in Eq. (33) and β_N not defined. Therefore, the angle β_N can be optimized using the SRP-only case. The solution for β_N is that in Eq. (23), and coincides to the one of Morgan [8]. This solution will be referred to as no-drag solution (NDS) in what follows.

The second observation is related to the semi-major axis constraint (Eq. (18)). It was shown that lift always comes with drag, and therefore in order to use a lift component to change the inclination, some drag is always generated. However, drag is opposite to velocity, and shall be compensated with an acceleration, directed towards the velocity, such that the net effect is no decrease of semi-major axis. This can only be provided by the SRP. However, it is possible to show that, in the part of the orbit when the spacecraft is traveling towards the Sun (i.e. $-\pi/2 < \alpha_\odot < \pi/2$), the optimal solution is always the NDS. Let us consider the optimistic case in which the Sun is below the orbital

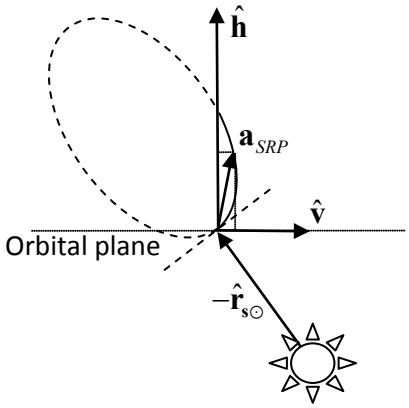

Fig. 10 Ellipse representing the possible SRP accelerations for each sail orientation (adapted from Ref. [11]). It shows that the orientation that maximizes the out-of-plane component satisfying the semi-major axis constraint is the one with the sail normal perpendicular to the velocity vector.

plane, and upwards out-of-plane acceleration is required. Figure 10, adapted from Ref. [11], is in the plane that contains the velocity and angular momentum vectors; the sail acceleration vector, when the sail is tilted in this plane, describes the ellipse represented in the figure. The part of the ellipse represented with a dashed line is obviously not feasible, as the sail acceleration has an in-plane component against the velocity vector. The only feasible part is the one plotted with a continuous line, and it is clear that the maximum out-of-plane acceleration, is obtained when the sail normal is perpendicular to the velocity vector (i.e. $\alpha_N = \pi/2, 3\pi/2$ as in Eq. (33), and β_N found with Eq. (23)), and this is again the NDS. Therefore it can be concluded that in the fraction of the orbit where $-\pi/2 < \alpha_\odot < \pi/2$, regardless the altitude, the optimal solution is always the NDS. This also means that, for this part of the orbit, an analytic solution exists for the combined atmosphere and SRP case.

Finally, at high altitude, the atmosphere will have a negligible effect, and the optimal solution will resemble the SRP-only solution (Eq. (24)) whenever this solution satisfies the semi-major axis constraint, i.e. in the part of the orbit where $0 < \alpha_\odot < \pi/2$. In the other part, as stated before, the solution is the NDS.

To summarize: in the part of the orbit where $-\pi/2 < \alpha_\odot < \pi/2$, the optimal solution is

always the NDS, regardless the altitude, and the analytical solution is given by $\alpha_N = \pi/2, 3\pi/2$ and β_N as in Eq. (23). In the other part of the orbit, the solution is the NDS at low altitude, the SRP-dominated one (Eq. (24)) at high altitude, and a combination of the two at intermediate altitudes. For this region, numerical methods have to be used to find the optimal solution of the full constrained problem. Knowing when the NDS is the optimal solution, on any given point of an arbitrary orbit (not just a circular one) would avoid the use of numerical techniques when they are not needed, and so speed up the computation. However, no simple relationship was found to determine when the NDS dominates.

The work of Morgan [8] uses the NDS throughout the orbit, and therefore it does not include the atmospheric effects. Although this law is optimal for a part of the orbit, even when the atmospheric effects are considered, there is a loss of a_h which could be gained through the full solution, especially at high altitudes where the effect of the drag starts to be relatively low.

The different optimal solutions which may be obtained along an orbit are now shown. Considering circular orbits, of increasing $a_0/(0.5\rho v^2 A/m)$, such that this coefficient is constant along each orbit, and the angle $\alpha_\odot$ spans a full circle every orbit. For simplicity, it is also considered that either maximum a_h (positive) or minimum a_h (negative) are sought along the whole orbit. The analysis is performed in the half-orbit where the NDS does not hold, see Fig. 11. Furthermore, due to symmetry, it is possible to limit the study to the quadrant $\pi < \alpha_\odot < 3\pi/2$. Figure 12 represents, for the orbit quadrant under consideration, the different solutions. The three plots represent the cases in which the Sun is in the orbital plane, the Sun is out of the plane of 23.48 deg (for example when the orbit is equatorial at summer or winter solstices) and the out-of-plane force required is either in the same direction or in the opposite one. The figures confirm what was found previously: where the atmospheric acceleration prevails, the solution is the NDS. Then, there is an intermediate region in which the solution is partly the NDS and partly the complete solution. As the atmospheric acceleration falls, the full solution becomes similar to the SRP-dominated solution. Also note that, when the SRP is dominant, there is a fraction of the orbit near $\alpha_\odot = 3\pi/2$ where the NDS and the SRP-dominated solutions are similar. The three plots also highlight that the regions vary their size depending on $\beta_\odot$ and the required direction of a_h. Finally, note that the region which requires a full

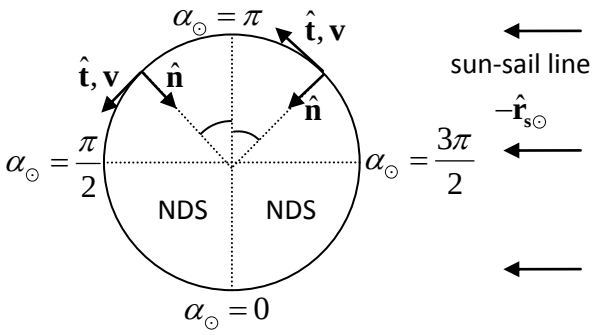

Fig. 11 For a circular orbit, symmetry in the half-plane where $\pi/2 < \alpha_\odot < 3\pi/2$.

numerical solution is, for a given sail in a circular orbit, limited to a narrow interval of altitudes.

For the case in Fig. 12(a) (i.e. $\beta_\odot = 0$), Fig. 13 shows the non-dimensional out-of-plane acceleration for four different values of $a_0/(0.5\rho v^2 A/m)$, and for the three solutions: NDS, full numerical and SRP-dominated. In these plots, the full solution always represents the highest value of acceleration that can be achieved, satisfying the constraints. However, it is interesting to note how this curve transforms, starting from NDS to SRP-dominated. Also note that the SRP-dominated solution is infeasible in some fractions of the orbit, due to $a_t < 0$.

V. Results

The control law defined in Sections III and IV is applied for a period of one year, starting from circular equatorial orbits. The motion of the Sun on the ecliptic is taken into account and the simulation starts in spring (i.e., at the beginning of the integration period the Sun is at its ascending node on the equatorial Earth-centred system). This implies that initially $\beta_\odot = 0$. The controlled equation of motion (Eq. (1)) is integrated and, at each instant of time, the optimal constrained sail attitude is computed, either analytically or through the numerical procedure described in Section III C. If the multi-start solver does not find a feasible solution (this may happen when the feasible region is extremely limited), then the NDS is used. This choice is made because the NDS is available analytically and guaranteed to be always feasible; furthermore, when the feasible region is small, the optimal solution is very close to the NDS.

Different initial orbit altitudes of 500 km, 600 km and 700 km and characteristic accelerations

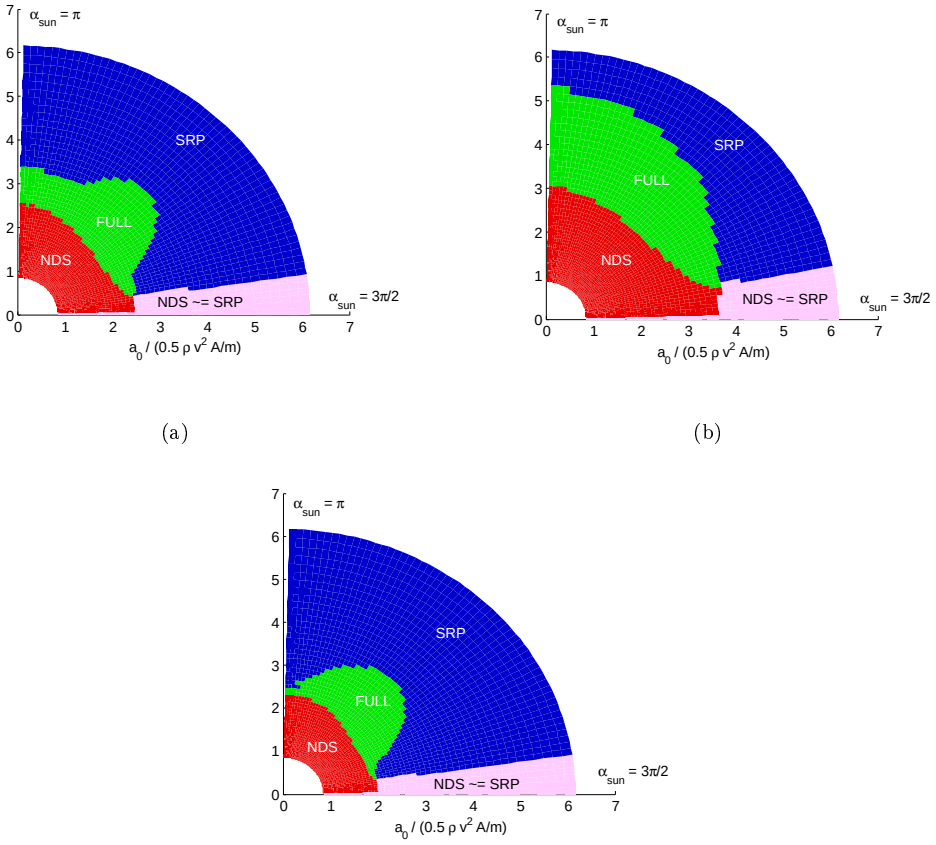

Fig. 12 Solution regions for circular orbits with different $a_0/(0.5\rho v^2 A/m)$ (radial direction) and for $\pi < \alpha_\odot < 3\pi/2$ (angular direction). (a) $\beta_\odot = 0$, $\max(a_h)$; (b) $\beta_\odot = 23.5$ deg, $\max(a_h)$; (c) $\beta_\odot = 23.5$ deg, $\min(a_h)$.

of the sail of 0.1 mm/s^2, 0.2 mm/s^2 and 0.3 mm/s^2 are considered to fully investigate the behavior in the region in which drag and SRP have comparing effects. Figure 14 represents the evolution of semi-major axis, eccentricity and inclination throughout the orbits for $a_0 = 0.2$ mm/s^2.

The three solution regions presented in Section IV are apparent. For example, considering the case starting at 500 km (line marked with '+'), for about 180 days, the NDS region is seen as there is no change in semi-major axis. The SRP-dominated solution region is then apparent starting approximately at 280 days since the launch date, as a linear increase in semi-major axis and an increased slope in the inclination evolution. The transition between the NDS and SRP-dominated cases belongs to the full solution region. As explained in Section IV, the difference is due to the

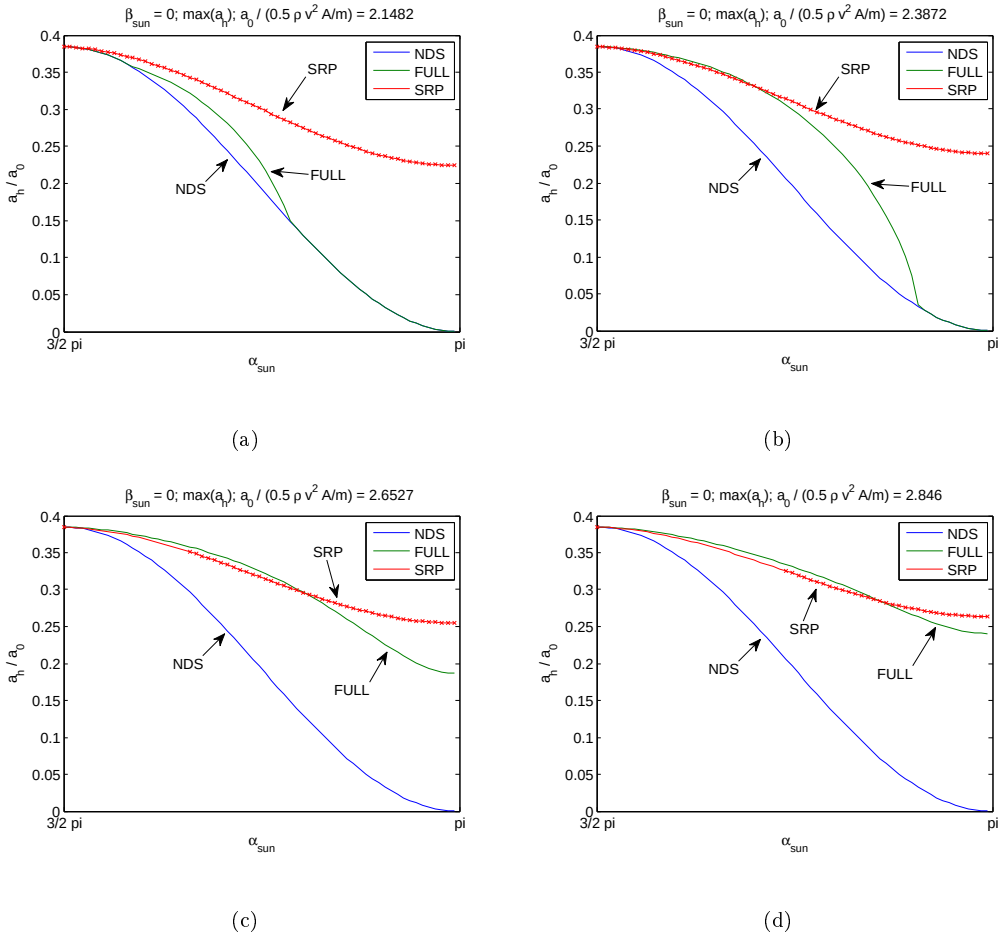

Fig. 13 a_h/a_0 **at for different values of** $a_0/(0.5\rho v^2 A/m)$**: (a) 2.1482; (b) 2.3872; (c) 2.6527; (d) 2.846. The NDS, the full solution and the SRP-dominated solution are represented with different lines in each plot. Crosses on the SRP solution show its infeasibility (due to** $a_t < 0$**).**

relative strength of SRP and aerodynamics effects. At lower altitudes, the control law must settle for the NDS ($\frac{da}{dt} = 0$) but as some fraction of the orbit is raised to higher altitudes (likely due to the increase in eccentricity), the control law is able to exploit the numerical solution and obtain the additional gain in the magnitude of a_h (hence higher inclination change), accompanied by $a_t > 0$.

The orbit evolution starting from a circular orbit at 600 km (dot-marked line in the figure) shows similar trends but, as expected, the SRP-dominated solution region is sooner reached. In the line for an orbit starting at 700 km (diamond-marked line), the immediate increase in semi-major axis followed by a quick transition into the linearly-increasing section suggests longer time in the SRP-dominated solution region, as would be expected for an orbit which starts at an altitude where

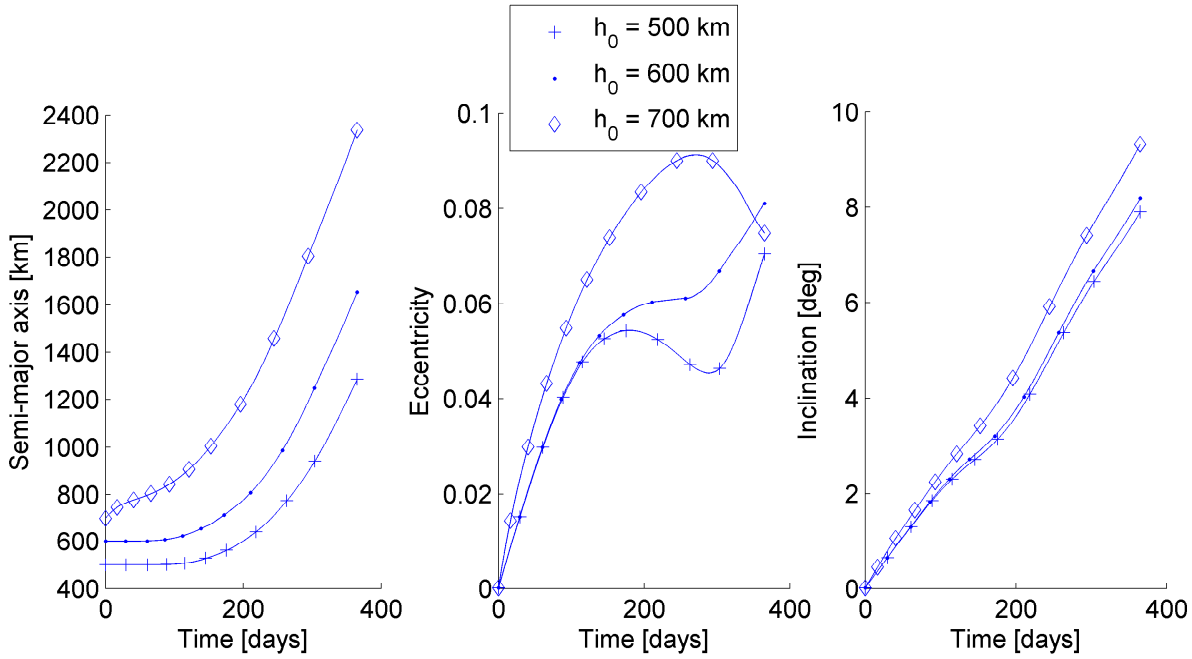

Fig. 14 Evolution of semi-major axis (a), eccentricity (b) and inclination (c) over one year, starting from circular equatorial orbits of different altitude. Characteristic acceleration $a_0 = 0.2\,\mathbf{mm/s^2}$

drag is less effective than SRP.

An insight into the time evolution of the eccentricity can be obtained from the analysis of the orbit evolution of a passively-stabilized attitude solar sail analysed in [6]. In this study, the sail is considered to always be maintained passively-oriented in the direction of the dominant perturbation; in other words, the cross sectional area with respect to SRP at high altitudes, or with respect to atmospheric drag at lower altitudes is considered constant. In this study the orbit evolution showed an interesting behavior in the $e - \phi$ phase space, where ϕ was defined as the angle between the orbit pericenter and the direction of the solar radiation. For an orbit close to the equatorial plane, $\phi \approx \Omega + \omega - (\lambda_\odot - \pi)$, where $\lambda_\odot$ is the angle measured on the ecliptic between the position of the Sun and the direction of the first point of Aries. The long-term secular evolution in the phase space showed a libration in $e - \phi$ around the equilibrium orbit at $\phi = 180$ deg due to the effect of SRP. Within the domain $\pi < \phi < 2\pi$ the eccentricity increases, for $0 < \phi < \pi$, instead, the eccentricity

decreases. The effect drag is superimposed to the libration causing a continuous decrease of the semi major axis.

The orbit evolution for the strategy described in Sections III and IV in Figure 15 shows some similarities with the passively-stabilized attitude solar sail [6]. It is possible to recognize an increase in eccentricity in the domain $\pi < \phi < 2\pi$, due to the exploitation of solar radiation pressure. In this case, with respect to the passively-stabilised sail, the control of the attitude of the sail allows the semi-major axis to be increased or to remain constant. Also, the lifting effect due the atmosphere is here exploited. However, it is still possible to observe a quasi-libration around the region close to $\phi = \pi$.

Although the final values of eccentricities at the end of the one-year integration period are still very close to zero, missions lasting multiple years may stray well away from circular, as the orbit is expected to librate around quasi equilibrium-orbits existing at higher value of the eccentricity for increasing semi-major axis. Moreover, due to periodic oscillations in eccentricity, if the staring altitude is low and the characteristic acceleration of the sail high, due to libration in eccentricity caused by SRP and a limited increase in semi-major axis, the perigee altitude will decrease and the orbit may evolve into a collision with Earth. Note that, since the libration is due to SRP, a higher maximum value of the eccentricity is reached for higher value of the characteristic acceleration of the sail. This is the case of the mission starting at a circular orbit at 500 km with $a_0 = 0.3\,\mathrm{mm/s^2}$, which impacts the Earth surface after about 100 days, as can be seen in Fig. 16.

In order to avoid an excessive increase of the eccentricity, the constraint in Eq. 18 could be modified to be $\frac{d(a(1-e))}{dt} \geq 0$, taking into account eccentric orbits, in a similar way to what is done in Ref. [3], where a constraint is added for orbit raising. Note that this problem was not faced in Ref. [9] as the initial orbit was considered to be perpendicular to the Sun radiation.

Table 1 reports the total increase in inclination and semi-major axis that can be archived over a one-year mission with a characteristic acceleration of $a_0 = 0.1\,\mathrm{mm/s^2}$, $a_0 = 0.2\,\mathrm{mm/s^2}$, and $a_0 = 0.3\,\mathrm{mm/s^2}$ subject to the control law for start altitudes of 500 km, 600 km, and 700 km.

As expected, a higher initial orbit and a higher characteristic acceleration of the sail allow a more consistent increase in eccentricity and semi-major axis. Considering the case with $a_0 = 0.2\,\mathrm{mm/s^2}$,

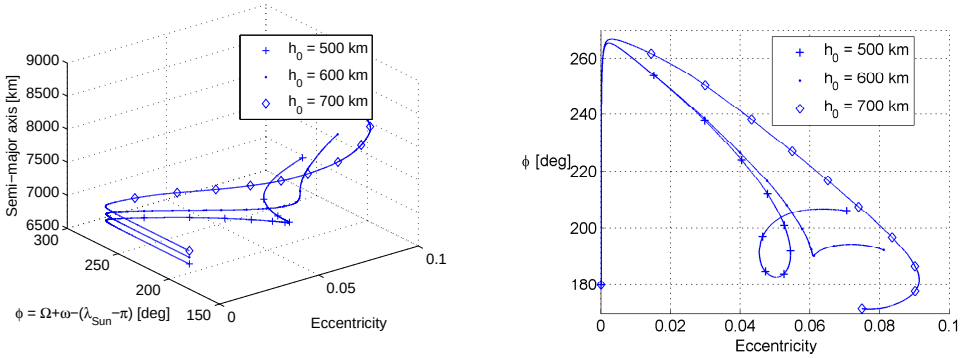

(a) (b)

Fig. 15 Evolution of eccentricity, sun-perigee angle and perigee altitude during the mission with characteristic acceleration of $a_0 = 0.2\,\mathrm{mm/s^2}$. (a) 3D view; (b) 2D view.

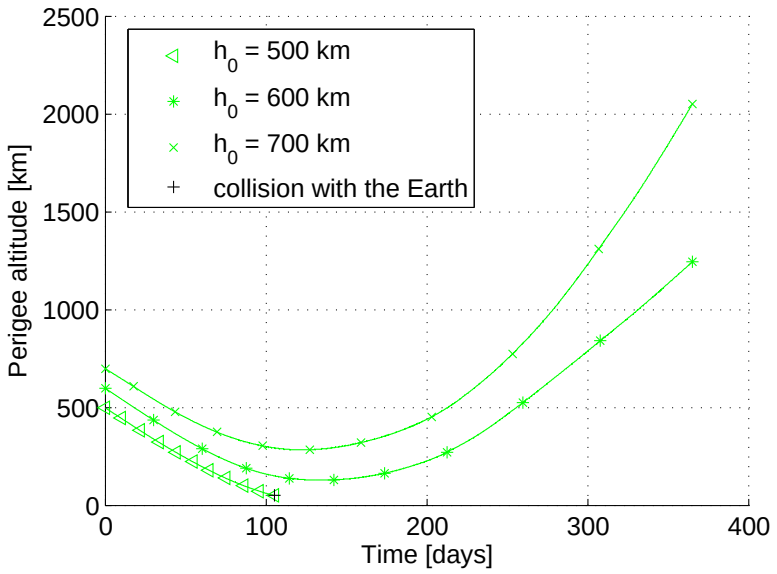

Fig. 16 Evolution of perigee altitude over one year, starting from circular orbits of different altitude. Characteristic acceleration of $a_0 = 0.3\,\mathrm{mm/s^2}$. Note that the spacecraft starting from 500 km impacts the surface of the Earth after about 100 days.

numerical results shows a total inclination changes of 7.9, 8.1 and 9.3 over a year for orbits starting at 500 km, 600 km and 700 km respectively. Each of the orbits experienced a significant increase in semi-major axis, ending the year at altitudes where SRP is the dominant force. The total change

Table 1 Total increase in inclination and semi-major axis for year-long missions with a sail with characteristic acceleration of $a_0 = 0.1\,\mathrm{mm/s^2}$, $a_0 = 0.2\,\mathrm{mm/s^2}$, and $a_0 = 0.3\,\mathrm{mm/s^2}$ subject to the control law for start altitudes of 500 km, 600 km and 700 km. Values with an asterisk (*) are at Earth impact.

	Inclination gain, deg			Semi-major axis gain, km		
	$0.1\,\mathrm{mm/s^2}$	$0.2\,\mathrm{mm/s^2}$	$0.3\,\mathrm{mm/s^2}$	$0.1\,\mathrm{mm/s^2}$	$0.2\,\mathrm{mm/s^2}$	$0.3\,\mathrm{mm/s^2}$
500 km	3.4968	7.8917	3.1713 (*)	56.4	786.55	12.937 (*)
600 km	4.0631	8.1803	12.4152	401.9	1053.9	1777.8
700 km	4.8803	9.3107	13.8496	828.2	1637.2	2526.5

of inclination shows approximatively a linear increase with initial altitude. As already pointed out, the case of characteristic acceleration of $a_0 = 0.3\,\mathrm{mm/s^2}$ and initial circular orbit at 500 km reach a small inclination change because the perigee altitude decreases below zero after about 110 days.

VI. Conclusion

In this work a solar sail spacecraft orbiting at low altitudes was considered. The effects of solar radiation pressure and aerodynamic forces were developed in a convenient model which allowed a description of all possible orientations of the sail in a three-dimensional space.

A control law was studied based on Gauss' equations to continuously increase the orbit inclination while maintaining no loss in semi-major axis. The optimal in-plane and out-of-plane angle of the sail for maximizing the instantaneous change in inclination can be found analytically in the case of solar radiation pressure only and was verified with previous literature. When the sail motion is dominated by atmospheric effects, a new analytical solution of the optimal angles of the sail was found. The case in which both solar radiation pressure and atmospheric effects have an influence on the orbit was solved numerically through a global optimization approach.

Through an analysis of the optimal solutions performed for a range of circular orbit altitudes, different values of the characteristic acceleration, and three possible value for the Sun's elevation with respect to the equator, it was possible to identify different regions of the solution domain. These regions correspond to different orbit regimes: one dominated by solar radiation pressure, one by

aerodynamics effects, and one where the effects of both perturbations are comparable. The results provided effective insight into two different solution regions: a no-drag region in which an analytical solution can be adopted, and a region in which numerical optimization is needed to determine an optimal solution.

Numerical results for a one-year-long mission, starting from circular equatorial orbits of 500, 600 and 700 km, show that a consistent increase in orbit inclination up to 14 degrees can be achieved with moderate characteristic accelerations of the sail ranging from 0.1 to 0.3 mm/s^2. All the solutions present resulted in a positive change in semi-major axis, allowing the spacecraft to reach the end of its mission at altitudes where solar radiation pressure is the dominant force. The results presented show that a short-term solar sail can be employed in the upper stages of the atmosphere for inclination and semi-major axis change manoeuvres.

Appendix

A. SRP-dominated case

In this appendix, we show the solution of Eq. (22), the non-feasible solution of system of Eqs. (16), and the limit case of Eq. (24).

Equation (22) can be re-written with the following notation: $A = \cos\beta_\odot, B = \cos(\alpha_\odot - \alpha_N), C = \sin\beta_\odot$, to obtain:

$$\cos\beta_N \left[AB\cos\beta_N + C\sin\beta_N\right] = 2\sin\beta_N \left[AB\sin\beta_N - C\cos\beta_N\right] \tag{35}$$

which, for $\beta_N \neq \pm\pi/2$, results in the quadratic form in $\tan(\beta_N)$:

$$\tan^2\beta_N - \frac{3C}{2AB}\tan\beta_N - \frac{1}{2} = 0 \tag{36}$$

which solves to:

$$\tan\beta_N = \frac{\frac{3C}{A} \pm \sqrt{\frac{9C^2}{A^2} + 8B^2}}{4B} \tag{37}$$

By noting that $\frac{C}{A} = \tan(\beta_\odot)$, the final result is:

$$\tan\beta_N = \frac{3\tan\beta_\odot \pm\sqrt{9\tan^2\beta_\odot + 8\cos^2(\alpha_\odot - \alpha_N)}}{4\cos(\alpha_\odot - \alpha_N)} \tag{38}$$

System of Eqs. (16) has a non-acceptable solution found inserting solution in Eq. (21a) into Eq. (23):

$$\tan\beta_N = \frac{3\tan\beta_\odot \pm\sqrt{9\tan^2\beta_\odot + 8\tan^2\beta_\odot\tan^2\beta_N}}{-4\tan\beta_\odot\tan\beta_N} \tag{39}$$

under the assumption that $\beta_\odot \neq 0$ and $\beta_N \neq 0$. This simplifies to:

$$\tan\beta_N = \frac{3 \pm\sqrt{9 + 8\tan^2\beta_N}}{-4\tan\beta_N} \tag{40}$$

or, for $\beta_N \neq 0$:

$$4\tan^2\beta_N + 3 = \pm\sqrt{9 + 8\tan^2\beta_N} \tag{41}$$

By squaring both sides and rearranging, one finds that the only real solution is $\beta_N = 0$, which cannot be accepted.

Finally, solutions of Eq. (24) at the limit are derived here. For the "-" solution:

$$\begin{gathered}\lim_{\beta_\odot\to\left(\frac{\pi}{2}\right)^-} \frac{3\tan\beta_\odot - \sqrt{9\tan^2\beta_\odot + 8}}{4} = \\ \frac{3}{4}\lim_{\beta_\odot\to\left(\frac{\pi}{2}\right)^-} \tan\beta_\odot\left[1 - \left(1 + \frac{8}{9\tan^2\beta_\odot}\right)^{\frac{1}{2}}\right]\end{gathered} \tag{42}$$

Considering the Taylor expansion, for $x \to 0$:

$$(1+x)^{\frac{1}{2}} = 1 + \frac{1}{2}x - \frac{1}{8}x^2 + ... \tag{43}$$

And substituting it into the argument of the limit:

$$\frac{3}{4}\lim_{\beta_\odot\to\left(\frac{\pi}{2}\right)^-} \tan\beta_\odot\left[-\frac{4}{9\tan^2\beta_\odot} + \frac{2}{9\tan^4\beta_\odot} + ...\right] = 0 \tag{44}$$

which means that $\beta_N = 0$. With the same procedure, for the "+" solution it is found that

$$\begin{aligned} &\lim_{\beta_\odot \to \left(\frac{\pi}{2}\right)^-} \frac{3\tan\beta_\odot + \sqrt{9\tan^2\beta_\odot + 8}}{4} = \\ &\frac{3}{4} \lim_{\beta_\odot \to \left(\frac{\pi}{2}\right)^-} \tan\beta_\odot \left[2 + \frac{4}{9\tan^2\beta_\odot} - \frac{2}{9\tan^4\beta_\odot} + ...\right] = +\infty \end{aligned} \tag{45}$$

and therefore $\beta_N = \pi/2$. Repeating the analysis for the case $\beta_\odot \to \left(-\frac{\pi}{2}\right)^+$ finds similar results.

B. Atmospheric effects-dominated case

The acceleration in h-direction due to aerodynamic lift is given by Eq. (29) as

$$a_{aero,h} = \frac{1}{2}\rho v^2 \frac{A}{m} \left(-2\cos\alpha_N \cos\beta_N \sin\beta_N \left(\sigma_n \left(v_b/v\right) + \left(2 - \sigma_n - \sigma_t\right) \left|\cos\alpha_N\right| \cos\beta_N\right)\right) \tag{46}$$

Firstly, restricted to the case of $\cos\alpha_N > 0$, the conditions for stationary point Eqs. (16a) and (16b) by substituting $a_{aero,h}$ in Eq. (46) give respectively:

$$\begin{cases} \left(\epsilon_1 + 2\epsilon_2 \cos\alpha_N \cos\beta_N\right) \sin\alpha_N \sin\left(2\beta_N\right) = 0 & \text{(47a)} \\ \cos\alpha_N \left(-2\left(\epsilon_1 + \epsilon_2 \cos\alpha_N \cos\beta_N\right) \cos\left(2\beta_N\right) + \epsilon_2 \cos\alpha_N \sin\beta_N \sin\left(2\beta_N\right)\right) = 0 & \text{(47b)} \end{cases}$$

where for clarity substituted $\epsilon_1 = \sigma_n \left(v_b/v\right)$ and $\epsilon_2 = 2 - \sigma_n - \sigma_t$ were substituted.

Equation (47a) gives the solutions

$$\epsilon_1 + 2\epsilon_2 \cos\alpha_N \cos\beta_N = 0 \tag{48a}$$

$$\sin 2\beta_N = 0 \tag{48b}$$

$$\sin\alpha_N = 0 \tag{48c}$$

Equation (48a) substituted in Eq. (47b) gives $\alpha_N = \pi/2$ for any value of β_N or $\beta_N = \pm\pi/2$ for any value of α_N. However, from Eq. (48a) this results in $\epsilon_1 = 0$ that is not a valid solution.

Equation (48b) instead gives $\beta_N = 0$, which substituted in Eq. (47b) gives $\alpha_N = \pi/2$ which is a trivial solution as the sail is traveling parallel with its attitude parallel to the velocity vector.

Finally, Eq. (48c) gives the solution $\alpha_{N,opt} = 0$ which substituted in Eq. (47b) is solved to

$$\cos\beta_{N,opt} = \frac{1}{18\epsilon_2}(-4\epsilon_1 + \frac{4\cdot 2^{1/3}(9\epsilon_2^2 + 2\epsilon_1^2)}{A} + 2^{2/3}A) \tag{49}$$

where

$$A = \left(135\epsilon_2^2\epsilon_1 - 16\epsilon_1^3 + 9\epsilon_2\sqrt{-288\epsilon_2^4 + 33\epsilon_2^2\epsilon_1^2 - 96\epsilon_1^4}\right)^{1/3} \tag{50}$$

Equation (49) is then manipulated through some algebraic and complex number manipulations to simplify the square root of a negative number and hence to eliminate any complex part through simplifications. The final result which contains only a real part is:

$$\cos\beta_{N,opt} = \frac{2}{9\epsilon_2}\left(-\epsilon_1 + \sqrt{2\left(9\epsilon_2^2 + 2\epsilon_1^2\right)}\cdot\cos\frac{\chi}{3}\right) \tag{51}$$

where the constant χ is defined as:

$$\chi = \arctan\frac{9\epsilon_2\sqrt{288\epsilon_2^4 - 33\epsilon_2^2\epsilon_1^2 + 96\epsilon_1^4}}{135\epsilon_2^2\epsilon_1 - 16\epsilon_1^3} \tag{52}$$

Note that the case with $\cos\alpha_N < 0$ is just anti-symmetric with respect to α_N and β_N as can be seen in Figure 5.

Acknowledgments

Part of the numerical simulations of this work were run on the Faculty of Engineering & ICSS High Performance Computer of the University of Strathclyde, Glasgow, UK. Camilla Colombo, Matteo Ceriotti and Colin McInnes would like to acknowledge the European Research Council, which funded their work as part of project 227571 VISIONSPACE at the University of Strathclyde. Valentin Stolbunov would like to acknowledge the University of Toronto Centre for International Experience, which funded his work as part of a research project abroad.

References

[1] Tsuda, Y., Mori, O., Funase, R., Sawada, H., Yamamoto, T., Saiki, T., Endo, T. and Kawaguchi, J.. Flight status of IKAROS deep space solar sail demonstrator. *Acta Astronautica*, 69(9Ũ10):833-840. 2011.

[2] McInnes, C. R.. Solar sail mission applications for non-Keplerian orbits. *Acta Astronautica*, 45(4 - 9):567 - 575. Third IAA International Conference on Low-Cost Planetary Missions. doi: 10.1016/S0094-5765(99)00177-0, 1999.

[3] Macdonald, M. and McInnes, C. R.. Analytical control laws for planet-centred solar sailing. *Journal of Guidance, Control, and Dynamics*, 28(5):1038-1048. doi: 10.2514/1.11400, 2005.

[4] Johnson, L., Whorton, M., Heaton, A., Pinson, R., Laue, G. and Adams, C.. NanoSail-D: A solar sail demonstration mission. *Acta Astronautica*, 68(5-6)2011.

[5] Lappas, V., Adeli, N., Visagie, L., Fernandez, J., Theodorou, T., Steyn, W. and Perren, M.. CubeSail: A low cost CubeSat based solar sail demonstration mission. *Advances in Space Research*, 48(11):1890 - 1901. doi: 10.1016/j.asr.2011.05.033, 2011.

[6] Colombo, C. and McInnes, C.. Orbital dynamics of 'smart dust' devices with solar radiation pressure and drag. *Journal of Guidance, Control, and Dynamics*, 34(6):1613-1631. doi: 10.2514/1.52140, 2011.

[7] Colombo, C., Lücking, C. and McInnes, C.. Orbit evolution, maintenance and disposal of SpaceChip swarms through electro-chromic control. *in press Acta Astronautica*, doi: 10.1016/j.actaastro.2012.05.035, 2012.

[8] Morgan, T.. The Inclination Change For Solar Sails and Low Earth Orbit. *Advances in Astronautical Sciences*, 79-104:559-573. 1979.

[9] Mengali, G. and Quarta, A. A.. Near-optimal solar-sail orbit-raising from low Earth orbit. *Journal of Spacecraft and Rockets*, 42(5):954-958. 2005.

[10] Storch, J. A.. Aerodynamic Disturbances on Spacecraft in Free-Molecular Flow. Technical Report TR-2003(3397)-1, The Aerospace Corporation, 2003.

[11] McInnes, C.. *Solar Sailing: Technology, Dynamics and Mission Applications*. Springer-Verlag. Berlin. 1999.

[12] Battin, R.. *An Introduction to the Mathematics and Methods of Astrodynamics*. American Institute of Aeronautics and Astronautics. Reston, VA. 1999.

[13] Vallado, D.. *Fundamentals of Astrodynamics and Applications*. Microcosm Press. Hawthorne, CA. 2007.